JOURNAL OF Applied Polymer SCIENCE

Special Issue: Microfiltration and Ultrafiltration Membrane Science and Technology

Guest Editors: Prof. Isabel C. Escobar (University of Toledo) and Prof. Bart Van der Bruggen (University of Leuven)

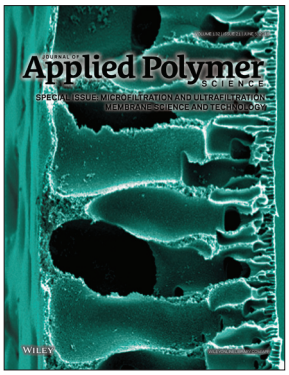

EDITORIAL

Microfiltration and Ultrafiltration Membrane Science and Technology
I. C. Escobar and B. Van der Bruggen, *J. Appl. Polym. Sci.* 2015, **DOI: 10.1002/app.42002**

REVIEWS

Nanoporous membranes generated from self-assembled block polymer precursors: *Quo Vadis*?
Y. Zhang, J. L. Sargent, B. W. Boudouris and W. A. Phillip, *J. Appl. Polym. Sci.* 2015, **DOI: 10.1002/app.41683**

Making polymeric membranes anti-fouling via "grafting from" polymerization of zwitterions
Q. Li, J. Imbrogno, G. Belfort and X.-L. Wang, *J. Appl. Polym. Sci.* 2015, **DOI: 10.1002/app.41781**

Fouling control on MF/ UF membranes: Effect of morphology, hydrophilicity and charge
R. Kumar and A. F. Ismail, *J. Appl. Polym. Sci.* 2015, **DOI: 10.1002/app.42042**

EMERGING MATERIALS AND FABRICATION

Preparation of a poly(phthalazine ether sulfone ketone) membrane with propanedioic acid as an additive and the prediction of its structure
P. Qin, A. Liu and C. Chen, *J. Appl. Polym. Sci.* 2015, **DOI: 10.1002/app.41621**

Preparation and characterization of MOF-PES ultrafiltration membranes
L. Zhai, G. Li, Y. Xu, M. Xiao, S. Wang and Y. Meng, *J. Appl. Polym. Sci.* 2015, **DOI: 10.1002/app.41663**

Tailoring of structures and permeation properties of asymmetric nanocomposite cellulose acetate/silver membranes
A. S. Figueiredo, M. G. Sánchez-Loredo, A. Maurício, M. F. C. Pereira, M. Minhalma and M. N. de Pinho, *J. Appl. Polym. Sci.* 2015, **DOI: 10.1002/app.41796**

LOW-FOULING POLYMERS

Low fouling polysulfone ultrafiltration membrane via click chemistry
Y. Xie, R. Tayouo and S. P. Nunes, *J. Appl. Polym. Sci.* 2015, **DOI: 10.1002/app.41549**

Elucidating membrane surface properties for preventing fouling of bioreactor membranes by surfactin
N. Behary, D. Lecouturier, A. Perwuelz and P. Dhulster, *J. Appl. Polym. Sci.* 2015, **DOI: 10.1002/app.41622**

PVC and PES-*g*-PEGMA blend membranes with improved ultrafiltration performance and fouling resistance
S. Jiang, J. Wang, J. Wu and Y. Chen, *J. Appl. Polym. Sci.* 2015, **DOI: 10.1002/app.41726**

Improved antifouling properties of TiO_2/PVDF nanocomposite membranes in UV coupled ultrafiltration
M. T. Moghadam, G. Lesage, T. Mohammadi, J.-P. Mericq, J. Mendret, M. Heran, C. Faur, S. Brosillon, M. Hemmati and F. Naeimpoor, *J. Appl. Polym. Sci.* 2015, **DOI: 10.1002/app.41731**

Development of functionalized doped carbon nanotube/polysulfone nanofiltration membranes for fouling control
P. Xie, Y. Li and J. Qiu, *J. Appl. Polym. Sci.* 2015, **DOI: 10.1002/app.41835**

JOURNAL OF Applied Polymer SCIENCE

Special Issue: Microfiltration and Ultrafiltration Membrane Science and Technology

Guest Editors: Prof. Isabel C. Escobar (University of Toledo) and
Prof. Bart Van der Bruggen (University of Leuven)

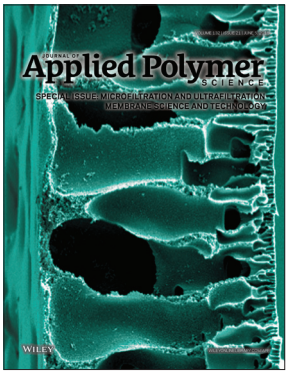

SURFACE MODIFICATION OF POLYMER MEMBRANES

Highly chlorine and oily fouling tolerant membrane surface modifications by *in situ* polymerization of dopamine and poly(ethylene glycol) diacrylate for water treatment
K. Yokwana, N. Gumbi, F. Adams, S. Mhlanga, E. Nxumalo and B. Mamba, *J. Appl. Polym. Sci.* 2015, **DOI: 10.1002/app.41661**

Fouling control through the hydrophilic surface modification of poly(vinylidene fluoride) membranes
H. Jang, D.-H. Song, I.-C. Kim, and Y.-N. Kwon, *J. Appl. Polym. Sci.* 2015, **DOI: 10.1002/app.41712**

Hydroxyl functionalized PVDF-TiO_2 ultrafiltration membrane and its antifouling properties
Y. H. Teow, A. A. Latif, J. K. Lim, H. P. Ngang, L. Y. Susan and B. S. Ooi, *J. Appl. Polym. Sci.* 2015, **DOI: 10.1002/app.41844**

Enhancing the antifouling properties of polysulfone ultrafiltration membranes by the grafting of poly(ethylene glycol) derivatives via surface amidation reactions
H. Yu, Y. Cao, G. Kang, Z. Liu, W. Kuang, J. Liu and M. Zhou, *J. Appl. Polym. Sci.* 2015, **DOI: 10.1002/app.41870**

SEPARATION APPLICATIONS

Experiment and simulation of the simultaneous removal of organic and inorganic contaminants by micellar enhanced ultrafiltration with mixed micelles
A. D. Vibhandik, S. Pawar and K. V. Marathe, *J. Appl. Polym. Sci.* 2015, **DOI: 10.1002/app.41435**

Polymeric membrane modification using SPEEK and bentonite for ultrafiltration of dairy wastewater
A. Pagidi, Y. Lukka Thuyavan, G. Arthanareeswaran, A. F. Ismail, J. Jaafar and D. Paul, *J. Appl. Polym. Sci.* 2015, **DOI: 10.1002/app.41651**

Forensic analysis of degraded polypropylene hollow fibers utilized in microfiltration
X. Lu, P. Shah, S. Maruf, S. Ortiz, T. Hoffard and J. Pellegrino, *J. Appl. Polym. Sci.* 2015, **DOI: 10.1002/app.41553**

A surface-renewal model for constant flux cross-flow microfiltration
S. Jiang and S. G. Chatterjee, *J. Appl. Polym. Sci.* 2015, **DOI: 10.1002/app.41778**

Ultrafiltration of aquatic humic substances through magnetically responsive polysulfone membranes
N. A. Azmi, Q. H. Ng and S. C. Low, *J. Appl. Polym. Sci.* 2015, **DOI: 10.1002/app.41874**

BIOSEPARATIONS APPLICATIONS

Analysis of the effects of electrostatic interactions on protein transport through zwitterionic ultrafiltration membranes using protein charge ladders
M. Hadidi and A. L. Zydney, *J. Appl. Polym. Sci.* 2015, **DOI: 10.1002/app.41540**

Modification of microfiltration membranes by hydrogel impregnation for pDNA purification
P. H. Castilho, T. R. Correia, M. T. Pessoa de Amorim, I. C. Escobar, J. A. Queiroz, I. J. Correia and A. M. Morão, *J. Appl. Polym. Sci.* 2015, **DOI: 10.1002/app.41610**

Hemodialysis membrane surface chemistry as a barrier to lipopolysaccharide transfer
B. Madsen, D. W. Britt, C.-H. Ho, M. Henrie, C. Ford, E. Stroup, B. Maltby, D. Olmstead and M. Andersen, *J. Appl. Polym. Sci.* 2015, **DOI: 10.1002/app.41550**

Membrane adsorbers comprising grafted glycopolymers for targeted lectin binding
H. C. S. Chenette and S. M. Husson, *J. Appl. Polym. Sci.* 2015, **DOI: 10.1002/app.41437**

Journal of Applied Polymer Science

Ultrafiltration of aquatic humic substances through magnetically responsive polysulfone membranes

Nur Atiah Azmi, Qi Hwa Ng, Siew Chun Low
School of Chemical Engineering Campus, Universiti Sains Malaysia, Seri Ampangan, 14300 Nibong Tebal S. P. S. Penang, Malaysia
Correspondence to: S. C. Low (E-mail: chsclow@usm.my or siewchun@gmail.com)

ABSTRACT: Organic foulants, such as humic acid substances, contribute to the irreversible fouling and flux decline in membrane separation processes. To reduce the membrane fouling potential, in this study, we explored the end-capping of functionalized nanostructured magnetite (Fe_3O_4) with poly(acrylic acid) (PAA) on the surface of the polysulfone (PSF) membrane. The binding stability of PAA-functionalized Fe_3O_4 [functionalized magnetite-responsive nanoparticles (F-MNPs)], combined with field emission scanning electron microscopy, energy-dispersive X-ray spectroscopy, and vibrating sample magnetometry, were studied to determine the deposited morphology and magnetic properties of F-MNPs on the membrane surface. In addition, the fouling analysis of the modified (F-MNPs-PSF) and unmodified (PSF) membranes were also being investigated through the filtration study. The results show that the magnetically responsive F-MNPs-PSF membrane developed in this study achieved high efficiency for the removal of humic substances when they were exposed to an oscillating external magnetic field. During filtration, the external magnetic field indirectly generated a torque that twisted the deposited Fe_3O_4 on the membrane surface. The actuated iron oxides consecutively reduced the concentration polarization around the top surface of the membrane and sequentially reduced the fouling propensity. These results provide some insight into the membrane's antifouling stability, which could be useful for environmental remediation. © 2015 Wiley Periodicals, Inc. J. Appl. Polym. Sci. **2015**, *132*, 41874.

KEYWORDS: hydrophilic polymers; magnetism and magnetic properties; membranes; morphology; nanoparticles; nanowires and nanocrystals

Received 18 July 2014; accepted 16 December 2014
DOI: 10.1002/app.41874

INTRODUCTION

The stringent regulations for drinking water quality have stimulated membrane filtration to become one of the best alternatives for replacing conventional drinking-water-treatment technologies.[1,2] Nevertheless, membrane fouling caused by the deposition of fouling materials on the membrane remains a critical issue in all applications of water filtration processes, and it restricts the widespread application of membranes. Fouling is a phenomenon that causes a rapid irreversible loss of flux through the membrane, which leads to the progressive deterioration of the membrane performance.[3]

In addition to membrane fouling issues, the feed water chemistry also plays an important role. Natural organic matter, such as humic substances, is one of the foulants present in surface or ground water.[4] Humic substances present in surface waters are typically found in the concentration range from 0.1 to 20 mg/L,[5] and in some cases, their concentration has been found to be as high as 30 mg/L.[6] Huge efforts have been focused on the role of several important properties of humic acid solutions.[7,8] For example, Jucker and Clark[7] found a greater humic acid (HA) adsorption on hydrophobic ultrafiltration (UF) membranes at low pH. The low pH was attributed to the reduction of net charged HA and formed aggregates in the solution. Thus, HA increased the solute adsorption capacity onto the membrane surface and formed a cake layer.[8]

In general, hydrophilic membranes exhibit lower levels of fouling and increased flux reversibility at their surfaces.[9] Many approaches have been carried out to improve the hydrophilicity of membranes, including modification of the membrane surface through polymerization, polyelectrolyte adsorption, or plasma modifications.[10,11] However, the modified polymer chain sometimes becomes highly swollen, and this leads to a decrease in the effectiveness of the membrane's mechanical properties.[11] Recent research attention has been paid to the development of nanocomposite membranes in which engineered nanoparticles

Additional Supporting Information may be found in the online version of this article.

are integrated into the porous membrane matrix to improve the membrane's antifouling performance.[12] For example, Teow *et al.*[12] investigated HA fouling with poly(vinylidene fluoride) (PVDF)/TiO_2 membranes. In their study, the PVDF/TiO_2 mixed-matrix membranes were less prone to HA deposition or better antifouling ability, as they exhibited a higher degree of hydrophilicity compared to the neat PVDF membrane.[12]

Among nanoparticles, ferromagnetic iron oxide (Fe_3O_4) has the longstanding interest of researchers because of its unique chemical and physical properties, low cost, low detection limit, and paramagnetism behavior.[13,14] Numerous studies have been reported about the fundamental scientific contributions of magnetite nanoparticles in water remediation,[15,16] heat-transfer enhancement, and biomedical applications.[17,18] One famous application of this magnetic material in environmental-related applications is the removal of organic and heavy-metal pollutants from water treatment processes.[19,20] In a study carried out by Hao *et al.*,[19] 98% of Cu^{2+} was successfully removed from polluted river and tap water through the direct magneto-electric properties of magnetite-responsive nanoparticles (MNPs).

However, it is a technological challenge to control the size, stability, and dispersability of nanoparticles. Magnetite nanoparticles tend to aggregate because of van der Waal's and magnetic dipole–dipole attractions to minimize the surface energies; this further produces a larger particle size and limited control size distribution. Moreover, bare MNPs are sensitive to oxidation in air, and this results in the loss of magnetism and dispersability.[21] Hence, the presence of an effective surface coating to retain the stability of MNPs is crucial. Practically, these protective layers will not only stabilize the MNPs but will also be used for further functionalization to achieve a good aqueous dispersion.[22,23]

Huang *et al.*[24] reported an approach to control the substructure of UF membranes by the combined effect of a magnetic filler and a parallel magnetic field. During membrane preparation, the magnetic Fe_3O_4 particles in the casting solution were arranged along the direction of a magnetic field. This oriented arrangement of the Fe_3O_4 gradually changed the membrane cross-sectional structure from a normal fingerlike macrovoid perpendicular to the membrane surface into a macrovoid structure parallel to the membrane surface; this further improved the membrane flux. Bhatt *et al.*[25] also prepared the PVDF–Fe_3O_4 composite films through the spin-coating method. However, SEM micrographs showed the aggregation of MNPs on the surface and within the porous PVDF matrix. Although the PVDF–Fe_3O_4 composite membrane demonstrated better flux performance, the aggregation kinetics and stability of the MNPs in the membrane matrices could not be controlled.

Therefore, in this study, we intended to develop a magnetically responsive polysulfone (PSF) membrane with a high magnetite binding stability on the membrane surface to improve the membrane antifouling ability under an oscillating external magnetic field. In this study, MNPs were first functionalized with the negatively charged poly(acrylic acid) (PAA) polymer to achieve a good aqueous dispersion. Different concentrations of the PAA functionalized magnetite-responsive nanoparticles (F-MNPs) were spin-coated on the surface of the PSF membrane. The dispersability of the MNPs and their binding stability on the membrane surface were elucidated. The magnetic properties of the F-MNPs were also investigated with vibrating sample magnetometry (VSM) to prove the magnetophoretic effect toward an external magnetic field. To further prove the functionality of this magnetically responsive nanocomposite membrane, filtration studies were carried out for the neat PSF membrane, the membrane coated with the negatively charged PAA polymer, and the membrane modified with the F-MNPs. The permeation and rejection performances for the HA foulant are discussed.

EXPERIMENTAL

Materials

The magnetite nanoparticles were supplied by NanoAmor. Different molecular weights of PAA (1.8, 450.0, and 3000.0 kDa), dimethylformamide (DMF), and HA were supplied by Sigma-Aldrich (St. Louis, MO). Sodium hydroxide (NaOH) and fuming 37% hydrochloric acid (HCl) were purchased from Merck (Darmstadt, Germany). In this study, PSF membranes with a molecular weight cutoff of 30,000 Da were supplied by GE Osmonic. All chemicals used were analytical-grade standards and were used without further purification.

Functionalization of the MNPs with PAA

MNPs (10 mg) with an isolated particle size of 7.0 nm were dispersed in 2 mL of DMF solution and ultrasonicated for 30 min to break up existing aggregations. Similarly, a solution with 200 mg of PAA at different molecular weights (1.8, 450.0, and 3000.0 kDa) was dissolved in 18 mL of DMF solution. The pH values of the Fe_3O_4 suspension and PAA solution were adjusted to 5 before the latter was added dropwise into the former solution. The physisorption of PAA on Fe_3O_4 via electrostatic attraction was allowed to occur for 1 day on an end-to-end rotating mixer. The F-MNPs were then collected with a permanent magnet and prewashed to remove excess PAA from the F-MNPs. The collected F-MNPs were dispersed and kept in 20 mL of deionized water; this rendered a 500-ppm F-MNP suspension. Dynamic light scattering (Zetasizer Nano ZS900, Malvern Instruments, Ltd., United Kingdom) was used to determine the hydrodynamic diameter and ζ potential of the F-MNPs. A light scattering from a laser beam ($\lambda = 633$ nm) was operated in the backscattering mode at an angle of 173°. The amount of PAA coated onto the MNPs surface was analyzed with thermogravimetric analysis (TGA; PerkinElmer Instruments, model STA 6000) recorded at a heating rate of 10°C/min from 0 to 800°C under a nitrogen atmosphere. The tests were carried out under a nitrogen flow to prevent the possibility of a weight increase as a result of iron oxidation.[21] The amount of PAA coated on the MNPs was calculated on the basis of eq. (1) for the PAA weight loss found at around 250–260°C:

$$\text{Amount PAA coated}\left(\frac{\text{mg}}{\text{g}}\right)\text{MNPs} = \frac{\text{TGA weight loss(\%)}}{100 - \text{TGA weight loss(\%)}} \times 1000 \quad (1)$$

Preparation of the Magnetite Nanocomposite Membranes

A flat-sheet PSF membrane that served as the support membrane was placed onto a glass plate fitted onto the vacuum

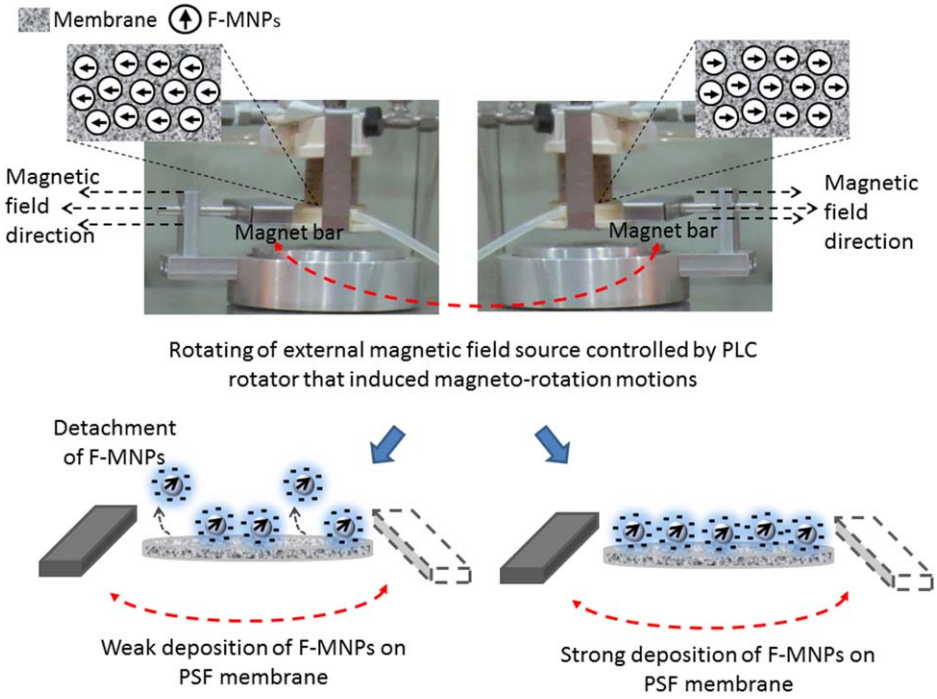

Figure 1. Schematic diagram for F-MNPs detachment analyses. Positioning of the magnetic field source controlled by a PLC rotator by either pointing the north poles to or away from each other. [Color figure can be viewed in the online issue, which is available at wileyonlinelibrary.com.]

chuck of the spin coater (Interscience G3P-8). Subsequently, 0.5 mL of F-MNPs suspension (500, 1000, or 2500 ppm) was dispersed on the PSF support membrane and spin-coated at a spinning speed of 3000 rpm with a rotation time of 10 s. The fluid was spun off the edges of the substrate until a desired homogeneous thin-film magnetophoretic polymer was formed. The dispersion procedure was done three times until a total of 1.5 mL of F-MNPs suspension was coated and spun off on each F-MNPs-PSF membrane. The membrane morphologies of all of the modified membranes were observed with field emission scanning microscopy (FESEM)/energy-dispersive X-ray spectroscopy (EDX; Zeiss SUPRA 35VP, Germany) at an accelerating voltage of 5 kV with platinum (Pt) coated before characterization.

Binding Stability of the F-MNPs onto the PSF Membrane

The binding stability of the magnetic responsive F-MNPs thin-film composite on the support PSF membrane was determined through the detachment (flush-out) analyses. First, the magnetically responsive PSF membrane was immersed in 20 mL of deionized water for 45 min. With the assistance of the programmable logic controlled (PLC) controlled rotator to change the position of the magnet filed source every 20 s, the magneto-induced rotation motions aligned the F-MNPs in a single direction at the specific interchange position. Subsequently, the promotion of the magnetophoretic actuation of F-MNPs on the membrane surface occurred; this could happen in two opposing directions, as shown in Figure 1. In this study, the magnetic field strength of the external magnetic bar was analyzed with a gauss meter (model GM-2) at various distances, as illustrated in the Supporting Information (Figure S1). As shown in Figure S1, the minimum oscillating magnetic field exposed to the iron oxide was found at 203 Gauss for a distance of 35 mm away from the external magnetic field source. This distance (35 mm) was referred to as the most far away position for the effective membrane area from the external magnetic bar. By changing the positioning of the magnetic field source controlled by the PLC rotator every 20 s (as illustrated in Figure 1), the oscillating magnetic field exposed to the iron oxide generated the actuation motions (vibration) on the membrane surface. Through the actuation motions of iron oxides, the weakly bound F-MNPs on the PSF membrane were probably be washed off. The detachment amount of the F-MNPs from the PSF membrane was then analyzed with an ultraviolet–visible spectrophotometer (Pharo 300 Spectroquant, Darmstadt, Germany) at 500 nm through comparison to the MNPs standard curve. On the other hand, the strongly bound F-MNPs on the PSF membrane sequentially endorsed the detachment of foulants that deposited on the membrane surface.

Magnetization Study

VSM [MicroSense model 8810 (10NRM), ADE Technologies] was used to characterize the magnetic properties of the F-MNP–PSF composite membrane. Two different F-MNPs-PSF concentrations of 500 and 2500 ppm were first freeze-dried before VSM analysis. The samples were placed in a nonmagnetic plastic tubular holder, and a magnetic field up to 20 kOe was applied.

Evaluation of the Membrane Antifouling Behavior

A concentration of 15 ppm of HA solution prepared at pH 7.5 ± 0.1 was used as the model natural organic matter. The addition of 1 mmol of calcium chloride ($CaCl_2$) into the HA feed solution was done to form a tighter bridge between the membrane surface and HA through the formation of calcium–

Table I. Amount of PAA Coated onto the F-MNPs

PAA molecular weight (kDa)	Weight remaining (wt %)	Mass of PAA grafted onto the MNPs (mg/g of MNPs)
1.8	53.20	12.13
450.0	48.95	16.73
3000.0	20.05	18.17

humic complexes.[26] All of the filtration experiments were conducted in a 25 mm diameter dead-end stirred cell (model 8010, Millipore Corp., Bedford, MA) with an effective membrane area of 4.1 cm^2 connected to an ultrapure-grade nitrogen-pressurized 1-L solution reservoir. Filtration was performed for 7 h with the operating pressure fixed at 0.5bar. All filtrations were carried out in at least three replicates, and the average filtration results are reported.

To investigate the magnetophoretic actuation functionality of the magnetically responsive PSF membrane, a magnetic field rotator fabricated in-house and connected to a permanent magnetic bar and a PLC rotator was used, as described in Figure 1. During membrane filtration, the PLC controlled rotator was set to change the position of the magnet field source every 20 s. The oscillating magnetic field exposed to the Fe_3O_4 generated the mechanical actuation motions of Fe_3O_4 on the membrane surface. By then, this helped us align the MNPs in a single direction at the specific interchange position; this sequentially endorsed the detachment of the foulants from the membrane. At the same time, a membrane surface coated with 1.8-kDa PAA without MNPs underwent the same filtration process to exclude the antifouling effects contributed by the negatively charged PAA. The PAA-coated PSF membrane was prepared according to the amount of PAA polymer wrapped around the F-MNPs and calculated on the basis of the TGA results (Table I).

RESULTS AND DISCUSSION

Development of the Magnetically Responsive PSF Membrane

Stability is of the utmost importance in the storage of ferrofluids. MNPs can easily aggregate and form large clusters because of their hydrophobic surfaces with large surface area-to-volume ratios. Ideally, the isolated nanoparticles coated on the membrane surface enhance the overall distribution and are easier for actuation when the nanoparticles are subjected to an external magnetic field. Thus, PAA was used to passivate the surface of the iron oxide nanoparticles to prevent agglomeration or gently break up the clusters of particles. As shown in Figure 2, the bare MNPs had hydrodynamic diameters of 376.7 ± 90.4 nm. Generally, the F-MNPs with different molecular weights of PAA showed lower hydrodynamic diameters (Figure 2). The stabilizing mechanism proposed here made a partition of the carboxyl groups of PAA[27] wrapped around the surface wall of the MNPs. The polymers' carboxylic groups were exposed around the surface of the MNPs when the PAA polymer was physisorbed to the MNPs colloids. In this case, the presence of negatively charged PAA on the F-MNPs surface wall enhanced the steric and electrostatic repulsions, and this prevented the agglomeration of particles. The steric stabilization factor induced by this coated polyelectrolyte strongly dictated the colloidal stability and led to a decrease in their hydrodynamic diameter.[28]

The lowest hydrodynamic diameter of 180.0 ± 14.2 nm was obtained as the lowest molecular weight of PAA (1.8 kDa) was used to passivate the surface of the iron oxide; this was almost two times lower than that of the bare MNPs. This indicated that the 1.8-kDa molecular weight of PAA was enough repulsive force to overcome the attractive forces acting on the MNPs. Because the PAA polymer compositions were kept constant at 200 mg throughout this study, the increases in the PAA molecular weight increased the viscosity of the suspension. A higher viscosity enhanced the formation of a dense layer, which wrapped around the surface of iron oxide. Thus, MNPs that were functionalized with PAA with 450.0- and 3000.0-kDa molecular weights demonstrated larger hydrodynamic diameters of 268.7 ± 61.2 and 289.3 ± 55.4 nm, respectively. In fact, these PAA dense layers at 450.0 and 3000.0 kDa gave some adverse effects, where the colloids' stability was affected by the chain length of the polymer. The chained-up effects caused by the longer chain of PAA at higher molecular weights (450.0 and 3000.0 kDa) might have interacted with more than one iron oxide particle. The polymers began to bridge between the particles and attract each other by the strong carboxylic groups to form a bigger cluster.[29] This explained why the larger hydrodynamic diameter of the F-MNPs was observed when the higher molecular weight of PAA was used (Figure 2).

The assessment of the compositional analysis of the F-MNPs was quantified with TGA. F-MNPs functionalized with 1.8, 450.0, and 3000.0 kDa of PAA demonstrated mass changes at the decomposition temperature of PAA (260°C) with remaining weights at 53.20, 48.95, and 20.05 wt %, respectively (Table I). The masses of PAA coated on the MNPs was calculated on the basis of eq. (1) and were found to be 12.13, 16.73, and 18.17 mg of PAA/g of MNPs, respectively. A markedly greater mass of the PAA polymer was coated on the MNPs when a higher molecular weight of PAA was applied. This result was in accordance with the previous discussion about the variation of

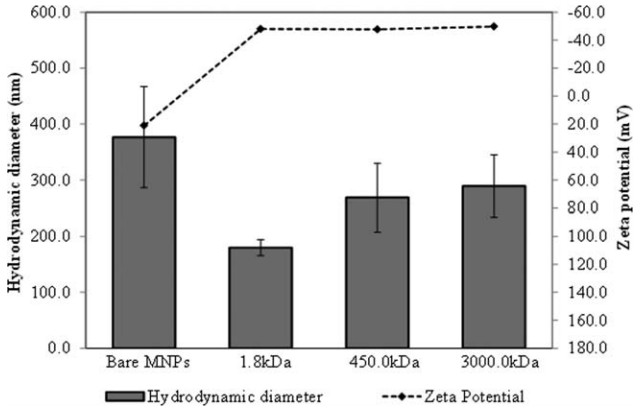

Figure 2. Hydrodynamic diameter and ζ potential values of F-MNPs functionalized with different molecular weights of the PAA polymer (at pH 5).

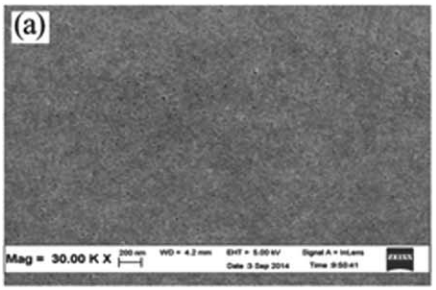

(e)

Element	Wt%	At%
C K	80.40	87.29
O K	11.62	09.47
S K	07.98	03.24

*Wt% = Normalized weight % concentration,
At% = Normalized atomic % concentration

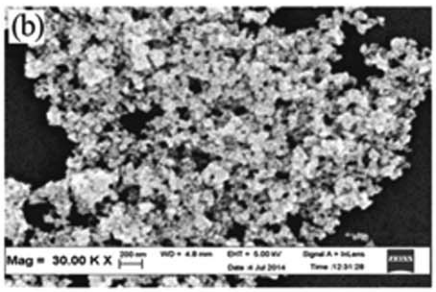

(f)

Element	Wt%	At%
C K	49.81	72.75
O K	13.66	14.97
S K	03.46	01.89
FeK	33.08	10.39

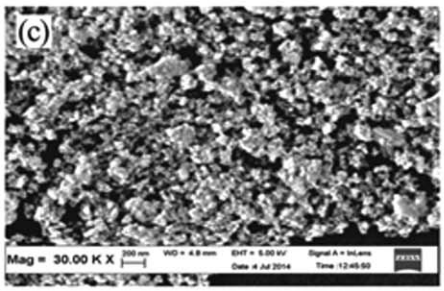

(g)

Element	Wt%	At%
C K	37.76	63.18
O K	15.25	19.15
S K	02.82	01.77
FeK	44.18	15.90

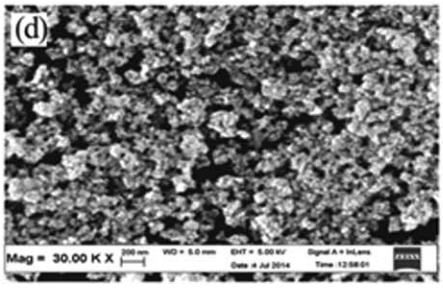

(h)

Element	Wt%	At%
C K	21.84	44.56
O K	18.98	29.08
S K	01.22	00.93
FeK	57.96	25.43

Figure 3. FESEM surface images and EDX spectra of the (a,e) neat PSF membrane, (b,f) 500 ppm F-MNPs-PSF (c,g) 1000 ppm F-MNPs-PSF and (d,h) 2500 ppm F-MNPs-PSF composite membranes.

the PAA polymer long chain and the polymer density on the surface of the MNPs.

The F-MNPs should have provided not only good compatibility of carboxyl groups toward MNPs but should have also retained the magnetic characteristics of MNPs for further application. The magnetic properties of F-MNPs were examined by measurement of the ζ potential for both bare and PAA F-MNPs. Figure 2 shows that the bare MNPs carried a positive surface charge of 21.1 ± 0.6 mV at pH 5. When the negatively charged PAA carboxylic groups were physisorbed around the surface of the MNPs, the ζ potential of the F-MNPs changed to a negative value. All of the F-MNPs exhibited similar ζ potential values, that is, -48.1, -47.8, and -49.8 mV with 1.8, 450.0, and 3000.0 kDa of PAA, respectively. It is worth noting that all of the F-MNPs achieved good colloidal stability with a ζ potential larger than -30.0 mV. In this study, F-MNPs functionalized with 1.8 kDa of PAA were chosen for further filtration study because they appeared to have the lowest hydrodynamic diameter, which was retained in the colloidal metastable region of -48.1 mV.

Figure 3 illustrates the surface morphologies of the neat PSF [Figure 3(a)] and F-MNPs-PSF composite membranes [Figure 3(b–d)] modified with different concentrations of magnetite nanoparticles. As shown, the neat PSF membrane [Figure 3(a)] demonstrated a clean and smooth surface, whereas the magnetically responsive F-MNPs-PSF composite membranes illustrated

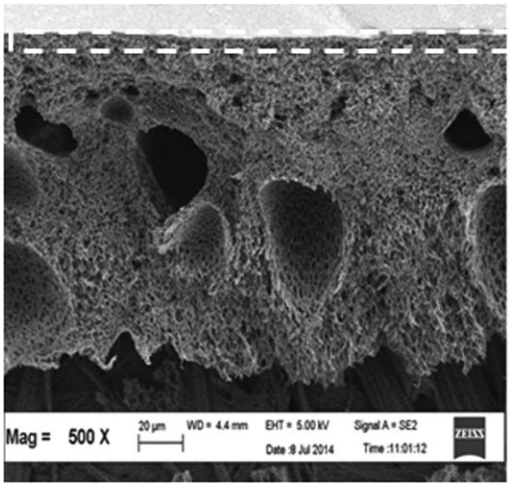

Element	Wt%	At%
C K	82.64	90.71
O K	06.14	05.06
S K	09.04	03.72
FeK	02.18	00.51

Figure 4. FESEM cross-sectional image and EDX spectra of the F-MNPs-PSF composite membrane.

rougher surfaces [Figure 3(b–d)]. The existence of Fe_3O_4 on the magnetically responsive PSF membranes were confirmed by EDX scanning, whereby Fe element was not detectable on the surface of the neat PSF membrane [Figure 3(e)], but additional Fe element was detected at the scanned membrane areas of the F-MNPs-PSF composite membranes (33.08, 44.18, and 57.96 wt % Fe for the initial F-MNPs disposition concentration of 500, 1000, and 2500 ppm, respectively). A single iron oxide nanoparticle consists of three elements of Fe and four elements of O. Thus, we expected to observe an increase in the weight percentage of O elements for those magnetite-responsive composite membranes [Figure 3(f–h)]. In addition, 57.96 wt % Fe was found on the membrane surface [Figure 3(h)], but only 2.18 wt % Fe was discovered when we scanned through the membrane cross-sectional area (Figure 4). These findings confirmed that the F-MNPs did not penetrate into the substructure of the membrane but were distributed on the membrane surface. In fact, the distribution of the Fe_3O_4 on the membrane surface helped to align the F-MNPs in the same direction when an external magnetic field was applied. The vibration of the MNPs was induced when opposing magnetic fields were alternately applied. This magneto-induced rotation of the F-MNPs during membrane filtration further promoted the detachment of foulants from the membrane surface.

Hypothetically, increasing the MNPs concentration enhanced the intensity of magnetophoretic actuation on the membrane surface. The existence of the higher actuation intensity of the F-MNPs may have increased the membrane vibration, and this promoted a higher detachment of HA foulants from the membrane surface. This detachment assisted in the reduction of the polarization concentration on the membrane surface and prolonged the lifespan of the membrane. However, this was workable when the required binding strength existed between the F-MNPs and PSF membrane. F-MNPs detachment tests were carried out to evaluate the binding stability of F-MNPs on the surface of the PSF membrane under an oscillating external magnetic field. Table II demonstrates the detachment level of F-MNPs from the PSF membrane surfaces. The results show that the 2500 ppm F-MNPs-PSF membrane that contained the highest amount of nanoparticles demonstrated the lowest detachment level of F-MNPs with only 1.54% or 4.70 µg of F-MNPs nanoparticles detached from the PSF membrane surface (Table II). These results led us to consider the formation of a semi-interpenetrating network of PAA-functionalized nanoparticles on the PSF membrane surface. [11] Theoretically, at a higher amount of F-MNPs, more PAA polymer would be used to functionalize the magnetite nanoparticles. The branching PAA polymer wrapped around magnetite nanoparticles would further associate with the PSF polymer network, and this resulted in the formation of a networklike structure.[30] Thus, the better binding strength linked the F-MNPs and the PSF membrane.

Figure 5 shows the magnetism properties of the composite membranes loaded with different amounts of F-MNPs. As shown in Figure 5, the coated 2500-ppm F-MNPs on the PSF membrane exhibited a saturation magnetism (M_s) of 9.80 emu/g; these were considered to have high magnetism properties[31,32] for actuation motions. The lower M_s properties found in composite F-MNPs-PSF membrane as compared to the pure colloidal F-MNPs sample (at approximately 55.00 emu g^{-1} [33] and 62.80 emu g^{-1} [34]) was due to the nonmagnetic properties of

Table II. Detachment of F-MNPs from the PSF Membrane Surface Under an Oscillating External Magnetic Field

Membrane	Initial mass of the coated F-MNPs (µg)	Detachment mass of the F-MNPs (µg)	Detachment of the F-MNPs (%)
500-ppm F-MNPs-PSF	60.98	9.40	15.41
1000-ppm F-MNPs-PSF	121.95	9.40	7.70
2500-ppm F-MNPs-PSF	304.88	4.70	1.54

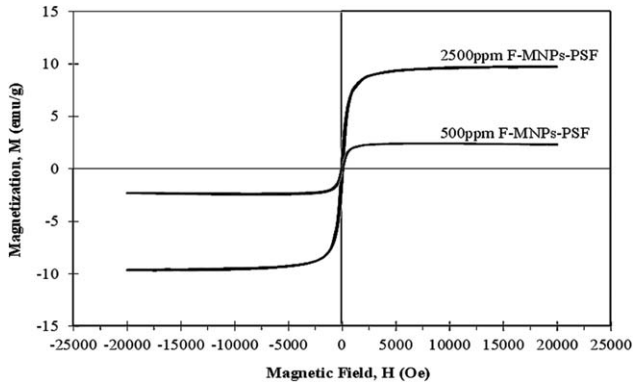

Figure 5. Magnetization curves of the 500- and 2500-ppm F-MNPs-PSF membranes.

the PSF membrane polymer in the sample. As expected, a lower M_s value was observed for the 500-ppm F-MNPs-PSF membrane (2.43 emu/g). This was due to the lower amount of F-MNPs deposited on the membrane surface, which thus caused lower magnetization.[35] Moreover, the low-remanent magnetization values (0.34 and 1.18 emu/g for 500- and 2500-ppm F-MNPs-PSF, respectively) found for both membrane samples suggested that only a low magnetic interaction existed between the particles; thus, a good dispersability of MNPs[36] existed when no external magnetic field was applied ($H = 0$). In this study, both of the F-MNPs-PSF membranes proved to have good magnetism properties. By changing the positioning of the magnetic field source controlled by a PLC rotator during the membrane filtration processes, the oscillating magnetic field exposed to the iron oxide generated the actuation motions (vibrations) on the membrane surface. The actuation motions of iron oxide sequentially endorsed the detachment of foulants that deposited on the membrane surface.

UF IN THE REMOVAL OF HA

In the absence of the F-MNPs composite layer, the neat PSF membrane [Figure 6(a)] exhibited serious extents of fouling at a steady-state normalized flux (J/Jo) of 29.0 ± 3.5%, although the initial flux (Jo) was shown to be high at 118.22 L m^{-2} h^{-1}. A relative flux decline profile was observed because of the concentration polarization phenomenon, which resulted from agglomerated HA clusters that attached to the surface of near-neutrally charged PSF membrane. Consequently, the neat PSF membrane was more severely fouled than the magnetically responsive F-MNPs-PSF composite membranes.

Through the introduction of the magneto-induced rotation motion, the magnetically responsive F-MNPs-PSF membranes showed better antifouling ability, whereas all of the membranes performed at a higher normalized flux (Figure 6). The relative changes in the normalized flux resulted from different degrees of magnetophoretic actuation of the F-MNPs that deposited on top of the composite membranes. With regard to the effects of the F-MNPs concentration, the high spin-coated concentration of the F-MNPs (2500 ppm) exhibited the highest attributions in mechanical magnetophoretic actuation motions of the F-MNPs to prevent the attachment of HA foulants (Figure 6). The normalized flux of the F-MNPs-PSF membrane was doubled (from 29.0 ± 3.5 to 47.0 ± 6.5%) when the membrane was operated under external magnetic field oscillation. The better resulting flux translated into sufficient actuation motions of the F-MNPs, which could successfully detach foulants near to the membrane surface. On the other hand, the low spin-coated concentrations of the F-MNPs (500 and 1000 ppm) demonstrated less actuation functionality of magnetite nanoparticles to reduce membrane fouling. As for the rejection performances, the HA rejection for all of the filtrations was shown to be high, above 80%. Again, these results confirmed that the detachment of the foulants from the membrane surface were dependent on the actuation effect created by the individual F-MNPs nanoparticles under an external oscillating magnetic field.

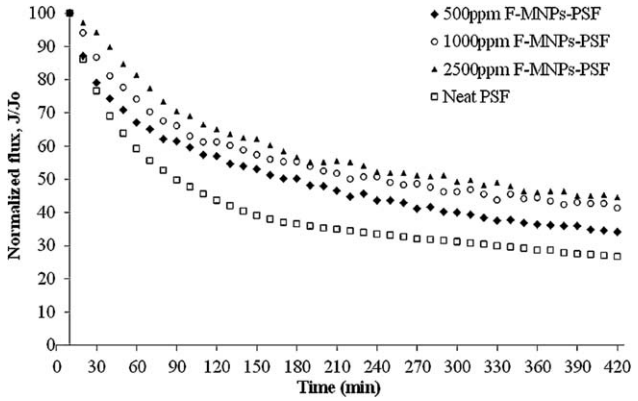

Figure 6. Normalized filtrate flux for the filtration of the 15 mg/L solutions of HA in the membrane fouling process. Jo is the initial permeation flux and J is the permeation flux at the ith time interval.

In fact, the modulation of the surface wettability of the PSF membrane by the adsorption of the hydrophilic and negatively charged PAA polymer was also a dominant factor that caused the membranes to foul comparatively less than the neat PSF membrane (Figure 7). To prove the effectiveness of the magnetophoretic actuation in reducing membrane fouling, the PAA-coated PSF (PAA-PSF) membrane was prepared and underwent the same filtration process. As expected, the hydrophilic and negatively

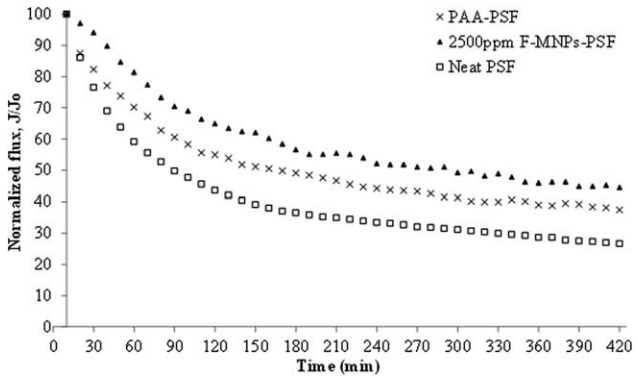

Figure 7. Comparison of the normalized filtrate flux values for the neat PSF, PAA-coated PSF, and magnetically responsive F-MNPs-PSF membranes for the filtration of 15 mg/L solutions of HA in the membrane fouling process. Jo is the initial permeation flux and J is the permeation flux at the ith time interval.

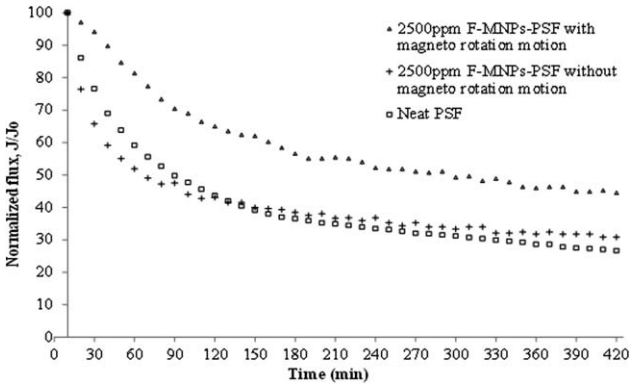

Figure 8. Comparison of the normalized filtrate flux values for the neat PSF and magnetically responsive F-MNPs-PSF membranes without and with magnetorotation motion for the filtration of 15 mg/L solutions of HA in the membrane fouling process. Jo is the initial permeation flux and J is the permeation flux at the ith time interval.

charged PAA-PSF membrane demonstrated less fouling (higher normalized flux at 39.0 ± 3.1%) than the neat PSF membrane.[37] In fact, the negatively charged PAA produced a Stern layer on the membrane surface. This Stern layer prevented the deposition of HA particles with similar negative surface charges. Hence, a higher membrane permeability was obtained. Because of the existence of the magnetite (Fe_3O_4) nanoparticles on the membrane surface, the negatively charged and hydrophilically modified F-MNPs-PSF membrane, which was originally susceptible to fouling, showed greater resistance to fouling because of the externally applied magnetic field and subsequent actuation of the magnetic nanoparticles (Figure 7). This is an important and significant result that proved the feasibility of the magnetically responsive F-MNPs in reducing membrane fouling.

A filtration test with the 2500-ppm F-MNPs-PSF membrane under conditions without an oscillating external magnetic field was also carried out, as presented in Figure 8. The filtration test was used to confirm the dominant factor to detach humic foulants from the membrane surface; this was attributed to the magnetophoretic actuation of the F-MNPs through the oscillating external magnetic field. As shown in Figure 8, a lower normalized flux of 33.0 ± 2.9% was observed for the nonmagnetite rotating condition as compared to that of under magnetite rotating conditions with an external oscillating magnetic field (normalized flux of 47.0 ± 6.5%). This result explains that the successful detachment of HA foulants was due to the mechanical actuation motions of the F-MNPs. The magnetophoretic actuation mode imposed a torque around the F-MNPs nanoparticles. This induced a vibration of F-MNPs that eventually promoted the detachment of foulants from the membrane. This detachment assisted in reducing the polarization concentration on the membrane surface and prolonged the lifespan of the membrane.

CONCLUSIONS

In this study, a magnetically responsive F-MNPs-PSF UF membrane was developed to facilitate the detachment of HA foulants from the membrane surface. Before filtration, a good colloid stability of the PAA F-MNPs was successfully developed with 1.8-kDa PAA and end-capped to the surface of the PSF membrane. Overall, the F-MNPs thin-film composite layer imposed a negative surface charged onto the surface of the PSF membrane; this prevented the deposition of negatively charged HA substances. Furthermore, the introduction of an oscillating external magnetic field to the membrane assisted the magnetophoretic actuation of the F-MNPs on the PSF membrane. The actuation effects created by individual F-MNP nanoparticles sequentially reduced the concentration polarization that occurred around the top surface of the membrane and reduced the fouling propensity. On the basis of previous findings, a fair process of combining the membrane with mechanically actuation motions could be proposed for sustainable wastewater reclamation and optimum control of contaminants.

ACKNOWLEDGMENTS

The authors are grateful for the financial support granted by The Institution of Higher Education Fundamental Research Fund Scheme (FRGS) (contract grant number 6071251) and the Universiti Sains Malaysia (USM) Membrane Science and Technology Cluster.

REFERENCES

1. Fu, X.; Maruyama, T.; Sotani, T.; Matsuyama, H. *J. Membr. Sci.* **2008**, *320*, 483.
2. Mbuli, B. S.; Nxumalo, E. N.; Mhlanga, S. D.; Krause, R. W.; Pillay, V. L.; Oren, Y.; Linder, C.; Mamba, B. B. *J. Appl. Polym. Sci.* [Online early access]. DOI: 10.1002/app.40109. Published Online: Nov 20, 2013. http://onlinelibrary.wiley.com/doi/10.1002/app.40109/full. Accessed 24 May 2014.
3. Katsoufidou, K.; Yiantsios, S. G.; Karabelas, A. J. *J. Membr. Sci.* **2005**, *266*, 40.
4. Malinga, S. P.; Arotiba, O. A.; Krause, R. W. M.; Mapolie, S. F.; Diallo, M. S.; Mamba, B. B. *J. Appl. Polym. Sci.* **2013**, *130*, 4428.
5. Rodrigues, A.; Brito, A.; Janknecht, P.; Proença, M. F.; Nogueira, R. *J. Environ. Monit.* **2009**, *11*, 377.
6. Brum, M. C.; Oliveira, J. F. *Miner. Eng.* **2007**, *20*, 945.
7. Jucker, C.; Clark, M. M. *J. Membr. Sci.* **1994**, *97*, 37.
8. Shao, J.; Hou, J.; Song, H. *Water Res.* **2011**, *45*, 473.
9. Ng, Q. H.; Lim, J. K.; Ahmad, A. L.; Ooi, B. S.; Low, S. C. *Sep. Purif. Technol.* **2014**, *132*, 138.
10. Hamid, N. A. A.; Ismail, A. F.; Matsuura, T.; Zularisam, A. W.; Lau, W. J.; Yuliwati, E.; Abdullah, M. S. *Desalination* **2011**, *273*, 85.
11. Mbareck, C.; Nguyen, Q. T.; Alaoui, O. T.; Barillier, D. *J. Hazard. Mater.* **2009**, *171*, 93.
12. Teow, Y. H.; Ahmad, A. L.; Lim, J. K.; Ooi, B. S. *J. Appl. Polym. Sci.* **2013**, *128*, 3184.
13. Zhang, Q.; Thompson, M. S.; Carmichael-Baranauskas, A. Y.; Caba, B. L.; Zalich, M. A.; Lin, Y.-N.; Mefford, O. T.; Davis, R. M.; Riffle, J. S. *Langmuir* **2007**, *23*, 6927.
14. Guo, H.; Wyart, Y.; Perot, J.; Nauleau, F.; Moulin, P. *J. Membr. Sci.* **2010**, *350*, 172.

15. Crane, R. A.; Dickinson, M.; Popescu, I. C.; Scott, T. B. *Water Res.* **2011**, *45*, 2931.
16. Mak, S.-Y.; Chen, D.-H. *Dyes Pigments* **2004**, *61*, 93.
17. Nishio, K.; Ikeda, M.; Gokon, N.; Tsubouchi, S.; Narimatsu, H.; Mochizuki, Y.; Sakamoto, S.; Sandhu, A.; Abe, M.; Handa, H. *J. Magn. Magn. Mater.* **2007**, *310*, 2408.
18. Dong, F.; Guo, W.; Bae, J.-H.; Kim, S.-H.; Ha, C.-S. *Chem. Eur. J.* **2011**, *17*, 12802.
19. Hao, Y.-M.; Man, C.; Hu, Z.-B. *J. Hazard. Mater.* **2010**, *184*, 392.
20. Illés, E.; Tombácz, E. *J. Colloid Interface Sci.* **2006**, *295*, 115.
21. Mincheva, R.; Stoilova, O.; Penchev, H.; Ruskov, T.; Spirov, I.; Manolova, N.; Rashkov, I. *Eur. Polym. J.* **2008**, *44*, 615.
22. Mahdavian, A. R.; Mirrahimi, M. A.-S. *Chem. Eng. J.* **2010**, *159*, 264.
23. Ge, J.; Hu, Y.; Biasini, M.; Dong, C.; Guo, J.; Beyermann, W. P.; Yin, Y. *Chem. Eur. J.* **2007**, *13*, 7153.
24. Huang, Z.-Q.; Chen, L.; Chen, K.; Zhang, Z.; Xu, H.-T. *J. Appl. Polym. Sci.* **2010**, *117*, 1960.
25. Bhatt, A. S.; Bhat, D. K.; Santosh, M. S. *J. Appl. Polym. Sci.* **2011**, *119*, 968.
26. Meng, S.; Ye, Y.; Mansouri, J.; Chen, V. *J. Membr. Sci.* **2014**, *463*, 102.
27. Yu, H.; Cao, Y.; Kang, G.; Liu, J.; Li, M. *J. Appl. Polym. Sci.* **2012**, *124*, 123.
28. Ghosh, S.; Jiang, W.; McClements, J. D.; Xing, B. *Langmuir* **2011**, *27*, 8036.
29. Ditsch, A.; Laibinis, P. E.; Wang, D. I. C.; Hatton, T. A. *Langmuir* **2005**, *21*, 6006.
30. Yilmaz, G.; Toiserkani, H.; Demirkol, D. O.; Sakarya, S.; Timur, S.; Yagci, Y.; Torun, L. *J. Polym. Sci. Part A: Polym. Chem.* **2011**, *49*, 110.
31. Thu, T. V.; Sandhu, A. *Mater. Sci. Eng. B* **2014**, *189*, 13.
32. Homayoonfal, M.; Mehrnia, M. R.; Shariaty-Niassar, M.; Akbari, A.; Sarrafzadeh, M. H.; Fauzi Ismail, A. *Desalin. Water Treat.* [Online early access]. Published online 10 Jun 2014 DOI: 10.1080/19443994.2014.923202. http://www.tandfonline.com/doi/full/10.1080/19443994.2014.923202#tabModule.
33. Deng, Y.-H.; Wang, C.-C.; Hu, J.-H.; Yang, W.-L.; Fu, S.-K. *Colloids Surf. A* **2005**, *262*, 87.
34. Yan, H.; Yang, L.; Yang, Z.; Yang, H.; Li, A.; Cheng, R. *J. Hazard. Mater.* **2012**, *229–230*, 371.
35. Liao, M.-H.; Chen, D.-H. *J. Mater. Chem.* **2002**, *12*, 3654.
36. Chen, Y.; He, F.; Ren, Y.; Peng, H.; Huang, K. *Chem. Eng. J.* **2014**, *249*, 79.
37. Amnuaypanich, S.; Naowanon, T.; Wongthep, W.; Phinyocheep, P. *J. Appl. Polym. Sci.* **2012**, *124*, 319.